Optimization of a Micro Wind Power Turbine Composed of a Magnetic Gear and Bearingless Generators

Gereon GOLDBECK*, Edmund MARTH*, Valentin MATEEV**, Iliana MARINOVA** and Wolfgang GRUBER*

* Institute of Electric Drives and Power Electronics
Johannes Kepler University Linz, Austria
** Department of Electrical Apparatus
Technical University of Sofia, Bulgaria

Abstract

This paper presents the design and optimization of a machine concept combining a magnetic gear with two bearingless generators, specifically designed for micro wind turbines. This approach aims to address the challenges of efficient energy conversion at small scales by leveraging the advantages of both components. The magnetic gear enables transmission of mechanical power from low rotational speeds to higher speeds, thereby reducing the overall size of the turbine system. The bearingless generator offers maintenance-free operation, enhancing reliability and reducing operational costs. The study details the design principles, optimization strategies, and parameter selection to maximize performance. Through comprehensive simulations and analyses, the results demonstrate that the optimized system can achieve an overall efficiency of over 93%. The findings indicate that the proposed machine concept is suitable for micro wind turbine applications, providing a compact, efficient, and low-maintenance solution. The paper concludes with a discussion of the benefits, limitations, and future prospects.

Keywords: Bearingless Generator, High Speed, Magnetic Gear, Micro Wind Turbines, System Optimization

1. Introduction

In recent years, the demand for sustainable energy solutions has led to innovative advancements in renewable technologies. Among these, the micro wind turbine has emerged as a compelling option for harnessing wind energy on a smaller scale. Recent advancements in micro wind turbine technology have shown promising developments in the field of small-scale energy harvesting. Researchers have explored various aspects of miniaturizing magnetic power generators, focusing on challenges such as integrating high-performance materials, microscale core laminations, and efficient power converters [1]. Small wind turbines, categorized as micro (up to 1 kW), mid-range, and mini-turbines (20kW and larger), have seen improvements in aerodynamics, blade manufacturing, and microprocessor controls [2].

Furthermore, studies on the combination of a magnetic gear (MG) with a bearingless machine for high-speed, compact, and efficient machine systems can be reviewed in the literature. Kumashiro et al. [3] investigated integrating a bearingless motor (BLM) into a MG, addressing efficiency challenges at high speeds. Marth et al. [4] proposed a design with two BLMs levitating the high-speed shaft of a MG, enabling high power density. These innovations aim to overcome limitations of mechanical bearings in high-speed rotors, offering advantages such as reduced maintenance and intrinsic overload protection [5]. Bearingless motors and generators (BLGs) have been a focus of research for several decades, with various motor types, force modeling, and control methods explored [6].

Combining an MG with a BLG offers significant advantages, especially for micro wind turbine applications. The MG enables contactless torque transmission, eliminating mechanical wear and reducing maintenance, which is ideal for small, decentralized systems that are often installed in hard-to-reach or off-grid locations. The BLG further simplifies the design by integrating rotor suspension and electrical power generation, removing the need for conventional bearings and thereby reducing friction and mechanical complexity. This results in a compact, lightweight, and highly reliable system with low start-up torque, making it well-suited for low and variable wind speeds. Additionally, the contactless nature of

both components allows for a fully sealed and maintenance-free operation, increasing durability and performance in outdoor or harsh environments typical for micro wind turbine installations.

This article focuses in the design of a micro wind turbine, highlighting their unique advantages and growing appeal. With their ability to generate clean energy in both urban and rural settings, micro wind turbines not only contribute to reducing carbon footprints but also empower individuals and communities to take charge of their energy needs.

2. Motivation

The use of micro wind turbines is motivated by the growing need for decentralized, renewable energy solutions, particularly in remote, off-grid, or urban areas where large-scale wind installations are not feasible. These small-scale turbines provide a sustainable way to generate electricity locally, reducing dependence on centralized power grids and fossil fuels. They are especially valuable for powering homes, rural facilities, telecommunications equipment, or IoT devices in locations with consistent wind resources. Additionally, micro wind turbines contribute to energy resilience, support environmental goals by lowering carbon emissions, and can be integrated with other renewable sources like solar to form hybrid systems for reliable, clean energy supply.

Furthermore, the demand for efficient and sustainable solutions in the field of electric motors increased, prompting manufacturers to investigate into materials that can enhance performance while minimizing environmental impact. One such material that has gained attention is ferrite, which offers a compelling alternative to the widely used rare-earth neodymium-iron-boron magnets. This article delves into the motivations behind choosing ferrite materials for electric motors, highlighting their advantages in terms of cost-effectiveness, availability, and environmental sustainability. Furthermore, the increase in power density in micro wind turbines is a key aspect. The wind speeds for urban (Linz), countryside (lake Neusiedl) and mountainous (mountain in the Alps) areas are in the range up to approx. 15m/s, as illustrated in Fig. 1. The energy distribution over the wind speed v_w determined from the distribution of wind speeds over time is shown in Fig. 2. The identification of an optimal rotor speed for wind turbines is described in detail in [7] and can be applied here. However, in order to achieve an increase in the generator's power density, the rotor speed must be increased. The following section presents a machine concept that takes these aspects into account.

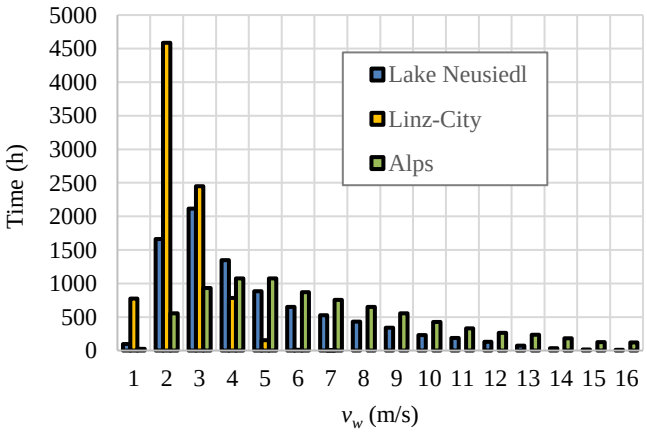

Figure 1: Wind speed over time for different areas.

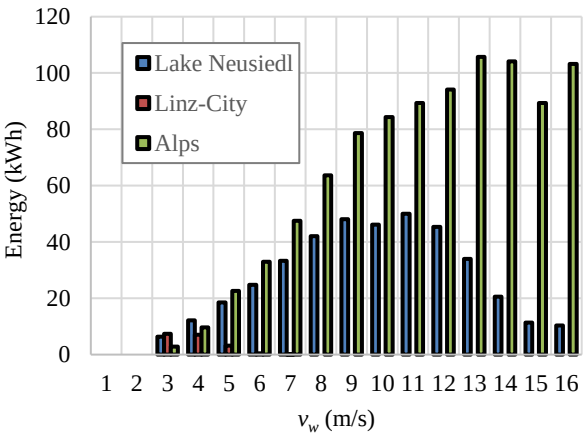

Figure 2: Energy distribution over the wind speed determined for different areas.

3. Machine Concept

The concept investigated here is based on the approach developed in [4], which combines a BLG with a MG for a micro wind turbine. In contrast to the conventional mechanical gearbox, a MG has the advantage that overloading for example due to sudden wind speed peaks, would not damage the MG. The magnetic gear can be operated near the stall torque with optimum efficiency by torque-controlling the BLG, which is implemented with a six-phase double layer winding. With this machine configuration consisting of two BLG and a centered MG, it is possible to significantly increase the outer rotor speed, which for the proposed application is in the range between 200 and 800 rpm, in order to achieve an increase in power density. The rotor blades are mounted directly on rotor R3 as shown schematically in

Fig. 3. Additionally, ferrites are used as permanent magnetic material for the MG and the BLG in order to reduce costs and ensure sustainability. The tip speed ratio λ (TSR) indicates how fast the wind turbine blade's tip is rotating relative to the speed of the wind and is a dimensionless number. Many investigations concerning optimum rotor TSRs can be found in literature [7], [8]. Generally, the optimal TSR for wind turbines typically falls within the range of 3 to 7. This range can vary depending on the specific design of the turbine, including for instance the number of blades [9].

To determine the speed and torque combination for different wind speeds for the machine concept to be optimized, some assumptions are made for a general estimate. Based on the groupings of wind turbines of different power classes described in [7], [9], [10], an optimum TSR (λ_{opt}) of 4 to 5 can be assumed here for a micro wind turbine with 3 rotor blades.

The power output of a micro wind turbine is generally calculated based on wind speed, the size of the blades, and the efficiency of the turbine [11], [12]. The basic equation to calculate the turbine output power P in W is equal to

$$P = \frac{1}{2} \cdot c_p(\lambda) \cdot \rho_{air} \cdot \pi \cdot r_R^2 \cdot v_w^3 \quad (1)$$

where $c_p(\lambda)$ is the power factor describing the conversion efficiency of wind energy into electrical energy, ρ is the air density (approximately equal to 1.225 kg/m at sea level), r_R is the radius for a circular rotor defined by the turbine blades given in m, and v_w is the wind speed in m/s, respectively. In literature, simplified approximation formulas based on wind speed, rotor area and other parameters to estimate the $c_p(\lambda)$ value for specific turbine types can be found. In practice, empirical models are often used to approximate the power factor $c_p(\lambda)$ as a function of TSR and the number of blades n. The power factor $c_p(\lambda)$ basically depends on the rotor speed and wind speed and reaches its maximum at a certain optimum wind speed. To approximate the curve of the power coefficient, the equation

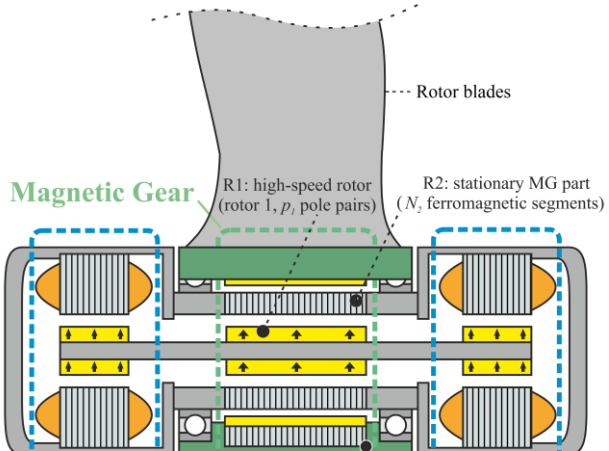

Figure 3: Machine schematics including BLG and MG.

$$c_p(\lambda) = c_{p,\max} \cdot \left(\frac{\lambda}{\lambda_{opt}}\right)^a \cdot e^{b \cdot \left(1 - \frac{\lambda}{\lambda_{opt}}\right)} \quad (2)$$

is often used in wind energy, where the parameters a and b affect the shape of the curve; a influences the gradient on the left side of the maximum, while b determines the width and the shape of the drop after the maximum. A specific example is described in [11] by Burton et al. The power curve of wind turbines is described using parametric models, whereby the parameters a and b as well as the maximum power $c_{p,\max}$ are adjusted in order to adapt the curve to the specific turbine.

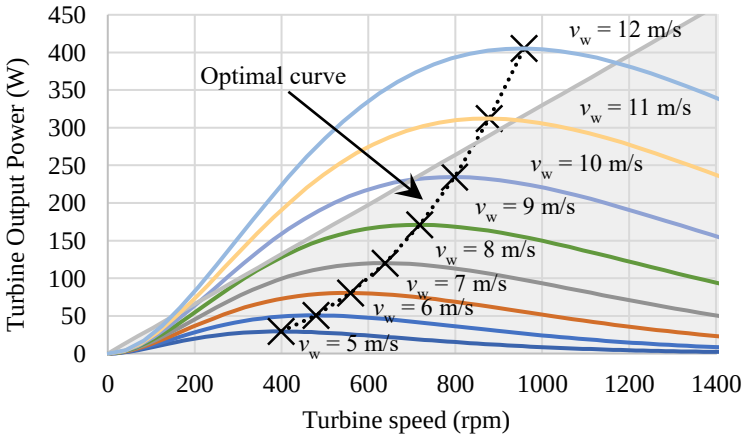

Figure 4: Turbine power output vs. speed

The power curve of a wind turbine shows how the turbine's power output varies with the rotor rotational speed (rotor speed). The approximation curves shown in Fig. 4 can be calculated using (1) and (2). Typically, as the wind speed increases, the turbine's power output also increases until it reaches a maximum, cf. 'optimal curve' in Fig. 4. Beyond this point, the power output levels off or slightly declines, which is often seen as a flat or gently declining section in the curve. The key factor for specifying the nominal rotor speed is not the wind speed itself, more important is the harvested energy, see Fig. 2. Thus, for the machine design a nominal rotor speed of 750 rpm is specified, which results from a wind speed

of 10 m/s (compare to Fig. 2), considering an optimal rotor tip speed ratio.

The MG is designed based on the tilting moment, which represents the maximum transmissible torque. Taking into account a safety factor of 10%, the tilting moment is determined from the load point corresponding to an optimal TSR value for a wind speed of 10 m/s, see Fig. 4. This wind speed corresponds to a rotor speed of 750 rpm. The resulting torque amounts to 3.3 Nm. The resulting limit characteristic for this maximum transmissible torque is indicated in Fig. 4 by the gray-shaded area.

Aligning the limit characteristic with a wind speed of 10 m/s offers the advantage that higher rotor speeds can also be achieved, albeit with lower torque. For example, at a wind speed of 12 m/s, the optimal TSR value cannot be reached; however, the characteristic curve remains very flat at higher rotor speeds, resulting in only a minimal reduction in the maximum turbine power. This means that even at increased wind speeds, the turbine can operate close to its maximum capacity with only slight performance losses.

4. Design Optimization

The machine concept is optimized using multi-objective optimization techniques. The design parameters and specifications of the machine concept optimization are described within this section. The subsequent optimization processes are introduced and the combinations of the separate optimizations are explained in detail. The results are then illustrated and finally a reasonable match of BLG and MG is selected.

4.1 Methodology and Specification

In the following, the methodology and the optimization parameters are introduced. A simplified approach is used, in which the MG and two BLGs (identical on both sides of the magnetic gear) are optimized separately. Finally, a suitable combination of MG and BLG is selected. To identify a favorable compromise between all, partly conflicting, criteria, the multi-objective optimizations are performed independently for each topology using a genetic algorithm and finite element simulations [13].

Table 1: Machine Configurations.

No.	p_1	N_2	p_3	G	n_1
#1	1	13	12	-12	-8700 rpm
#2	1	17	16	-16	-11600 rpm
#3	1	21	20	-20	-14500 rpm
#4	1	25	24	-24	-17500 rpm
#5	2	27	25	-12.5	-9100 rpm

The goal of optimizing this electric machine concept is to enhance its overall performance while meeting specific design constraints. The primary objectives are to achieve a high efficiency at the targeted load point, minimize the overall size of the machine, reduce the torque ripple of the rotor shaft, and require minimal current to levitate the magnetically supported rotor. It is essential to reach high overall power density. This means a reduction in losses and axial length. In addition to other criteria like destabilizing radial high-speed rotor stiffness, material costs are minimized.

One of the main difficulties lies in balancing these often-conflicting goals. For instance, increasing the magnetic flux to improve efficiency can lead to larger machine dimensions or higher levitation currents. Similarly, reducing the size of the machine might compromise the magnetic flux distribution or the levitation stability. Achieving a low levitation current while maintaining stable rotor suspension also requires careful design of the magnetic circuit and control strategies.

Table 2: Objective parameters for the optimization of MG and BLG.

Parameter	Description
η	Efficiency (of MG and BLG) → MAX
l_{fe}	Axial length to reach the desired torque (MG) → MIN
l_{s}	Axial length of stator with end-windings (BLG) →MIN
I_{s}	Stator phase current → MIN
$k_{b,x}$	Deflection-force factor (for MG and BLG) → MIN
$k_{b,i}$	Current-force factor → MAX
$x_{\varphi,f}$	Ratio of minimal to maximal radial force versus rotor angle → MAX
$thd(U_1)$	Total harmonic distortion of line-to-line voltage → MIN
m_{m}	Total mass of permanent magnets → MIN
$T_{r,\mathrm{R3}}$	Torque ripple of R3 → MIN
$T_{r,\mathrm{R1}}$	Torque ripple of R1 (for MG and BLG) → MIN

Various optimization processes have to be carried out separately to optimize this machine concept. As already mentioned, different gear

ratios of the MG are considered here. According to the load point definition presented in Sections 1 and 2, the respective basic machine configurations, see Table 1, are optimized separately. Finally, all objectives are listed in Table 2.

4.1.1 Magnetic Gear

Due to the different basic variants of the MGs with different gear ratios, correspondingly different nominal speeds result for the BLG. Thus, correspondingly adapted basic variants of the BLG must also be analyzed, which differ in load point definition. The parameterized model of the MG is illustrated in Fig. 5. The visualized various parameters can be varied during the optimization. Based on the machine concept described in Section 3, rotor R2 remains stationary, while rotors R1 and R3 rotate in a gear ratio according to Table 1. The fundamental principles for calculating the gear ratios can be taken from [14].

Again, the different basic variants are optimized separately. However, the same objectives and boundary conditions are applied to each of these basis variants.

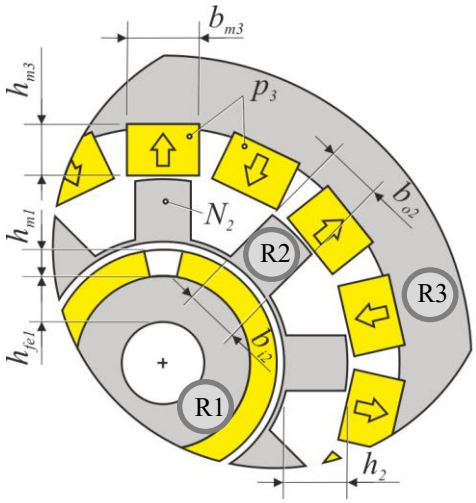

Figure 5: Schematic view of the parametric MG model.

4.1.2 Bearingless Generator

The optimization of a bearingless generator begins with the fundamental model, which features a six-phase winding system with a pitch factor of 3, as illustrated in Fig. 6. This configuration provides a robust basis for achieving high efficiency and reliable operation. The relatively high pitch factor slightly reduces torque generation but is necessary to achieve substantial radial suspension forces.

In Fig. 6, the various parameters that can be varied during the optimization process are visualized, allowing for a systematic exploration of the design space. Among these parameters, the winding number is also a key variable that influences the generator's performance characteristics. By adjusting these parameters, the design can be finetuned to maximize efficiency, minimize losses, and optimize the overall power output. This approach ensures that the bearingless generator is tailored to meet specific operational requirements, making it suitable for the proposed machine concept where compactness, reliability, and high performance are essential.

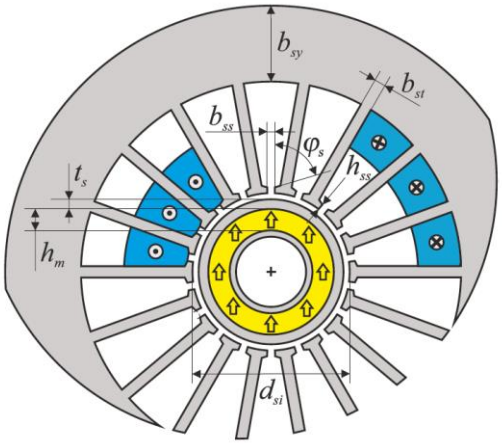

Figure 6: Schematic view of the parametric BLG model.

Moreover, the rotor pole pair number is equal to 1 to minimize losses that typically increase with higher speeds. Additionally, a bandage is applied around the rotor to provide extra mechanical stability and support during operation at elevated rotational velocities. The number of phases is set to six, as this is the minimum required for bearingless machines configured in a double-star arrangement, which allows for the generation of two independent rotating magnetic fields, one for torque production and another for the suspension force generation. Furthermore, a slot number of 18 is chosen because it ensures low harmonics and smooth, quiet operation, resulting in minimal torque ripple and a stable running behavior. The axial position of the rotor is passively stabilized from the generators and the bearing as well. The suspension force generation is also of central importance for the optimization. This is represented by the parameters $k_{b,x}$ and $k_{b,i}$, see Table 2.

4.2 Results

Figure 7a displays the efficiencies of the magnetic gear (vertical axis) and the bearingless motors (horizontal axis). The overall efficiency, denoted as η_t, which results from the combination of the magnetic gear (MG) and the bearingless motor (LBG), is illustrated with dashed lines for better clarity.

Initially, it becomes evident that achieving a total efficiency of 90% with the configuration using a four-pole MG rotor R1, corresponding to a gear ratio of G = −12.5, is not possible under the given boundary conditions. The same can also be found here for the variants with a gear ratio of G = −24. All other configurations can reach overall efficiencies exceeding 91%, with some even surpassing 93%. For selecting an appropriate topology, a minimum total efficiency of 92% should be maintained.

Furthermore, the current density, which arises due to the starting current, is of significant importance. Since the underlying machine concept does not include active cooling, the short-time lift-off current density should not exceed 50 A/mm, even if this occurs only temporarily. Figure 7b clearly shows that topologies with gear ratios of G = −12 and G = −20 deliver the best results in terms of low current density.

Another key parameter is the minimal spatial size of the machine. To evaluate this, Figure 7c presents the total axial length, comprising the lamination stack lengths of both the MG and the bearingless motor, as well as the length of the winding heads, relative to the magnet mass.

At first glance, the combination of the MG and the BLG with a gear ratio of G = −20 appears to be an ideal choice. This configuration achieves high efficiencies, and the variants with this gear ratio also perform well in terms of magnetic mass and space requirements. When selecting the most suitable variant from all the examined gear ratios, priority is given to overall efficiency, starting current, space requirements, and magnetic mass. Comparative analyses have shown that variants with a gear ratio of G = −12 tend to have a higher magnetic mass, while those with G = −16 feature a lower magnetic mass. The G = −12 variants, on the other hand, demonstrate very high overall efficiencies, but they also require more space, which is reflected in the increased total length of the system. Figure 7 illustrates the Pareto front of all the combinations, highlighting the trade-offs between these parameters. The optimal variant selected is marked in color and will be discussed in more detail in the following. This comprehensive evaluation helps in

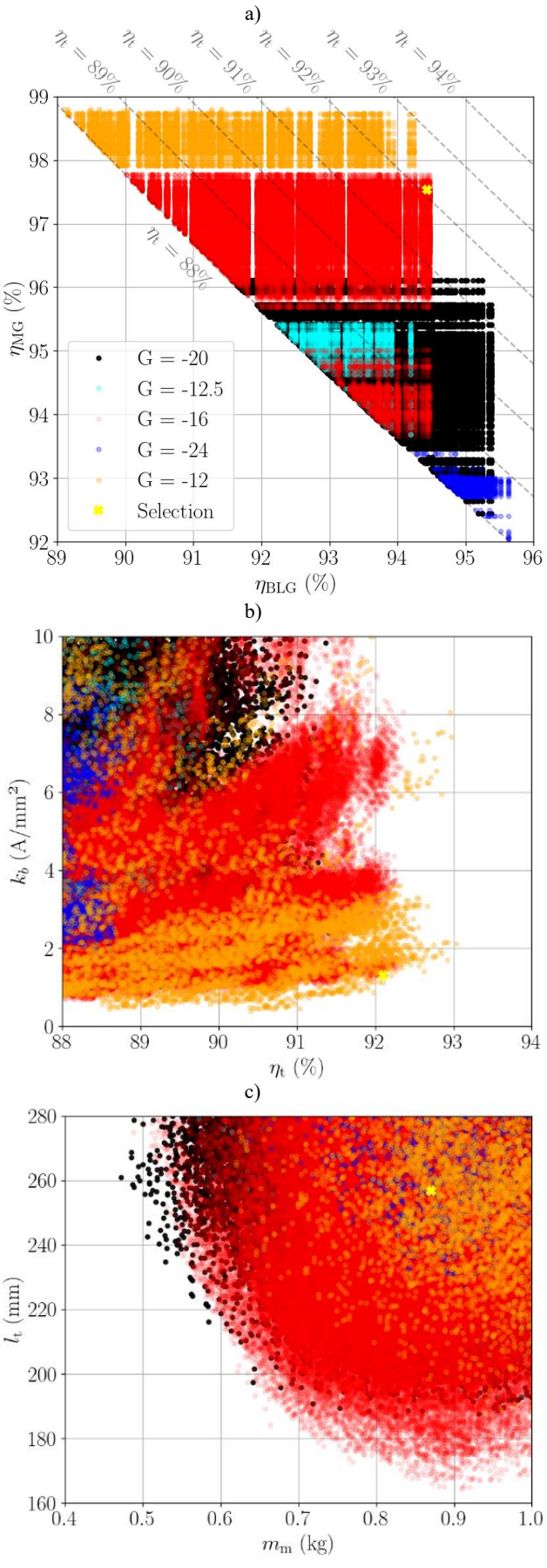

Figure 7: Optimization results – pareto front.

Table 3: Optimization results – geometry parameters and objectives.

Geometry parameters MG		Geometry parameters BLG		Objective	
Parameter	Value	Parameter	Value	Parameter	Value
h_{fe1}	9.24 mm	b_{ss}	1.3 mm	η	92.1%
h_{m1}	7.56 mm	b_{st}	2.5 mm	η_{MG}	97.53 %
b_{i2}	4.24 mm	b_{sy}	5.5 mm	η_{BLG}	94.43%
b_{o2}	3.0 mm	h_m	5 mm	l_{fe}	101.9 mm
h_2	3.97 mm	h_{ss}	1.6 mm	l_s	77.4 mm
b_{m3}	5.21 mm	φ_s	101°	I_s	1.19 A_{rms}
h_{m3}	3.07 mm	w_c	19	$k_{b,x}$	-8.57 N/mm
		d_{so}	80 mm	$k_{b,i}$	4.7 N/A
		d_{si}	37 mm	$x_{\varphi,f}$	0.966
		d_{ri}	10 mm	$thd(U_{ll})$	0.94 mV
		t_s	1.2 mm	m_m	0.87 kg
				$T_{r,R3}$	2.8%
				$T_{r,R1}$	1.3%

balancing efficiency, size, and magnetic mass to identify the best design tailored to specific application needs. A suitable selection represents a compromise between the key performance targets, particularly when considering a high overall efficiency and a compact machine design. In this context, an optimal gear ratio of G = -16 was identified, which achieves a total efficiency of 92.1%. The overall length of the machine is 256.7 mm, making it well-suited for the proposed application.

Furthermore, the optimization results indicate that the starting current for all examined variants can be reduced to an acceptable minimum, primarily due to the use of ferrite magnets with a remanent flux density of 0.42 T. The chosen design features a starting current density of 1.3 A/mm², which is close to the rated current I_s. Besides, at the nominal load point, a current density of 1.08 A/mm² is achieved, ensuring efficient operation under typical conditions.

The rotor torque ripple for both the MG and the BLG is sufficiently low, contributing to smooth and reliable operation. All geometric parameters associated with this optimal variant, as described in Figs. 5 and 6, are documented in Table 3. Additionally, the results for the key performance indicators can be found summarized in the same table, providing a comprehensive overview of the optimized machine design.

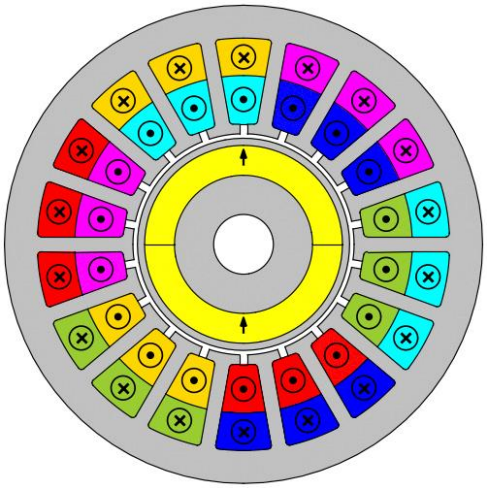

Figure 9: Optimized BLG model.

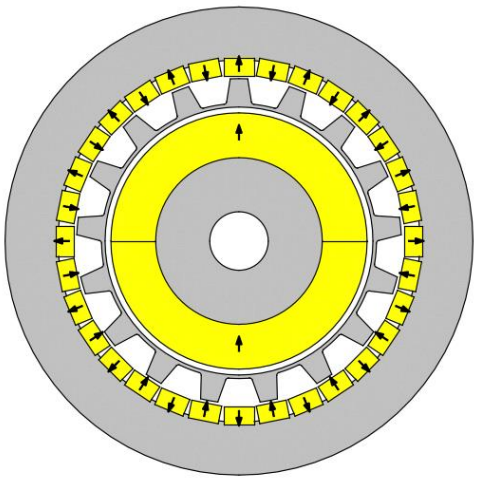

Figure 8: Optimized MG model with G = -16.

5. Conclusion and Outlook

This paper demonstrates the feasibility of a novel machine concept that combines an MG with a BLG for use in micro wind turbines. The integration of an MG is particularly advantageous because it can effectively handle the typical power curves observed in wind turbines, which often involve variable and fluctuating loads.

The study highlights that the proposed design can be implemented in small-scale wind energy systems, offering promising performance characteristics. The optimization processes achieved satisfactory results in terms of efficiency and performance, which are critical factors for the practical deployment of such turbines. The optimized configuration not

only improves the overall energy conversion efficiency but also reduces the required installation space, making it suitable for various applications, including urban or remote areas.

The authors plan to conduct more detailed analyses of the machine's performance across different wind speeds to better understand its behavior under varying environmental conditions. Moreover, a comparison will be made with a standard permanent magnet synchronous machine that has been optimized under the same boundary conditions. In addition, the study also shows that this application does not require very high gear ratios and therefore does not result in high rotational speeds. Further comparisons will be carried out to check whether generators with conventional bearings achieve equally satisfactory results. This will help to evaluate the relevance and potential advantages of implementing the machine concept presented here, by providing a clear benchmark against a conventional, well-established motor design. Finally, a prototype is to be developed to validate the theoretical and simulated results and enable further investigations.

Acknowledgment

This work has been supported by the COMET-K2 "Center for Symbiotic Mechatronics" of the Linz Center of Mechatronics (LCM) funded by the Austrian federal government and the federal state of Upper Austria.

References

[1] D. Arnold, "Review of microscale magnetic power generation. IEEE Tran. Mag.43(11): 3940-3951," *Magnetics, IEEE Transactions on*, vol. 43, pp. 3940 –3951, Dec. 2007.

[2] P. D. Clausen and D. H. Wood, "Recent advances in small wind turbine technology," *Wind Engineering*, vol. 24, no. 3, pp. 189–201, 2000.

[3] A. Kumashiro, A. Chiba, W. Gruber, W. Amrhein, and G. Jungmayr, "Investigation of a combined electromagnetic structure of bearingless motor and magnetic gear," in *2020 IEEE Energy Conversion Congress and Exposition (ECCE)*, 2020, pp. 278–284.

[4] E. Marth, W. Gruber, S. Mallinger, V. Mateev, and I. Marinova, "Magnetic-geared bearingless motor unit with central exterior output," Jun. 2024, pp. 1–6.

[5] A. Kumashiro, A. Chiba,W. Gruber,W. Amrhein, and G. Jungmayr, "Novel reluctance-type magnetic geared motor with integrated with high-speed bearingless motor," in *2022 International Power Electronics Conference (IPECHimeji 2022- ECCE Asia)*, 2022, pp. 1762–1768.

[6] B. Liu, "Survey of bearingless motor technologies and applications," in *2015 IEEE International Conference on Mechatronics and Automation (ICMA)*, 2015, pp. 1983–1988.

[7] M. Ragheb and A. M. Ragheb, "Wind turbines theory - the betz equation and optimal rotor tip speed ratio," in *Fundamental and Advanced Topics in Wind Power*, R. Carriveau, Ed., Rijeka: IntechOpen, 2011, ch. 2.

[8] M. Bechly, P. Clausen, P. Ebert, D. Wood, and A Pemberton, "Field testing of a prototype 5kw wind turbine," 1997.

[9] H. M. S. Murthy, R. N. Hegde, R. U. Gaonkar, and N. Rai, "A critical assessment of significant developments in wind turbine performance," *International Journal of Ambient Energy*, vol. 45, no. 1, p. 2 267 568, 2024.

[10] K. Adeyeye, N. Ijumba, and J. Colton, "The effect of the number of blades on the efficiency of a wind turbine," *IOP Conference Series: Earth and Environmental Science*, vol. 801, p. 012 020, Jun. 2021.

[11] T. Burton, D. Sharpe, N. Jenkins, and E. Bossanyi, *Wind Energy Handbook*. John Wiley & Sons, 2001, isbn: 9780471489979.

[12] J. Manwell, J. McGowan, and A. Rogers, *Wind Energy Explained: Theory, Design and Application*. Wiley, 2010, isbn: 9780470686287.

[13] S. Silber, W. Koppelstätter, G. Weidenholzer, G. Segon, and G. Bramerdorfer, "Reducing development time of electric machines with symspace," in *8th International Electric Drives Production Conference (EDPC)*, 2018, pp. 1–5.

[14] G. Jungmayr, J. Loeffler, B. Winter, F. Jeske, and W. Amrhein, "Magnetic gear: Radial force, cogging torque, skewing and optimization," in *2015 IEEE Energy Conversion Congress and Exposition (ECCE)*, 2015, pp. 898–905.